Numerical study on a multifracture enhanced geothermal system considering matrix permeability enhancement induced by thermal unloading

Peng Zhao [a], Jun Liu [b,*], Derek Elsworth [c]

[a] *State Key Laboratory of Geohazard Prevention and Geoenvironment Protection, Chengdu University of Technology, Chengdu, 610059, China*
[b] *Key Laboratory of Deep Underground Science and Engineering (Ministry of Education), Institute of New Energy and Low-Carbon Technology, Sichuan University, Chengdu, 610065, China*
[c] *Department of Energy and Mineral Engineering, EMS Energy Institute and G3 Center, Pennsylvania State University, University Park, PA, 16802, United States*

ABSTRACT

We explore an enhanced geothermal system (EGS) reservoir with horizontal wells connecting multiple hydraulic fractures. In particular we follow the implications of complex thermal–hydraulic–mechanical on the thermal unloading of rock matrix on the permeability evolution. The accuracy and reliability of the proposed model is validated/verified against an existing analytical solution and the Fenton Hill demonstration project. Then, the effect of the fracture number on the heat extraction process is discussed. Results show that matrix permeability enhancement induced by the thermal unloading should be considered in the coupling model. Compared with the results from the traditional model, the maximum temperature difference at the production well can reach 20 K. More fractures in the EGS are advantageous for expanding the cooling range along the production well and have a great impact on the temperature. Generally, an EGS with more fractures is prone to obtain a higher production temperature. In the EGS, fracture number plays an important role in considering both the heat transportation rate and the cooling range in a geothermal exploration process. Per the consideration of geothermal exploitation in the matrix and fracture, there is only a slight difference in the heat extraction ratio for the four numerical cases.

1. Introduction

Geothermal resources provide an attractive source of low/zero-carbon energy due to their cleanliness and significant reserves [1,2]. Non-hydrothermal resources are found in the subsurface where moderate/high temperature (150–650 °C) are co-located with low porosity and therefore little native water content. Generally, this type of hot dry rock (HDR) resource exhibits ultralow porosity and permeability (>microDarcy) which results in difficulty in geothermal energy production by heat transfer fluids [3]. Thus, reservoir manipulation to enhance the permeability of HDR is crucial to enable effective and economically viable heat extraction [4]. Since the demonstration of Fenton Hill as a potentially viable geothermal site, the extensive development of massive hydraulic fracturing for the recovery of shale gas has meant that this is a transferrable technology provided the issue of thermal short circuiting may be solved [5].

Although the feasibility of commercial heat extraction from EGS reservoirs has been confirmed by several demonstration projects [1], many difficulties remain unresolved with regard to commercial production. One critical issue is insufficient understanding of the full heat extraction process [6] and the strong and positive feedbacks. The recovery of geothermal resources from HDR resources involves several interactive physical processes, including heat exchange and transfer, fluid flow in the rock matrix and fractures, and rock deformation and failure. Furthermore, these processes are strongly coupled, typically described through thermal–hydraulic–mechanical coupling (THM) processes [1]. Once a fractured reservoir is created by hydraulic fracturing of hydraulic shearing, the interaction among the components of the THM process intrinsically controls the efficiency of heat extraction. Numerical simulation is one effective method to analyze the full heat extraction process. Coupled models have been used to study the characteristics of fluid flow, heat transfer and mechanical response in EGS reservoirs [6,7] and reservoirs below oilfields [8].

To further understand the factors affecting the efficiency of heat

---

extraction, various studies have investigated the issue to understand the relative impact of geological factors versus operating parameters. With regard to geological factors, the impacts of natural fractures have been explored [9,10] to define the impacts of permeability on heat recovery [11] and to understand the evolution of the SRV [12]. Conversely, operational are shown to have a nonnegligible role in thermal exploitation and are controllable. Principal controls are on well patterns, selection of working fluids and design of the injection schedule [1,13]. In addition, the impact on heat recovery of multilateral well EGS systems has been explored [11,14–17] as well as the impact of different well types and number of wells, alignment and placement on energy productivity. These impacts include the effect of the aperture, height, number, and spacing of artificial fractures on the heat extraction process [15,18–20]. Additionally, the selection of working fluids (water–based fluids and gas fluids) has also been studied. Taking CO_2 as the working fluid, several numerical simulations of heat extraction have also been performed [10,21–23], including both water and CO_2 as the working fluid in the numerical model [8,24]. The results showed that compared to using water in EGSs, utilizing CO_2 as the working fluid could improve heat recovery efficiency.

Currently, a series of numerical studies on heat extraction have been carried out. These models, to a degree, exhibit a complicated THM process. However, it is still a challenge to comprehensively consider the interactions between different physical processes. As cryogenic fluid is injected into HDR, the temperature difference between the rock matrix and the fluid can reach 100 °C or higher [1], thus generating thermal stress. Once the stress exceeds the critical value, thermal damage occurs in the rock matrix. In HDR, thermal damage has a great influence on its properties, especially its permeability [25–31]. For example, when a rock sample was cooled from 325 °C to 25 °C by cold water, its permeability was enhanced by more than one order of magnitude [28]. By evaluating cases with different constant permeabilities in the thermal–hydraulic numerical model, Han et al. [18] found that the permeability increasing of a stimulation reservoir favour reducing the injection pressure and increasing the mining efficiency. Additionally, the variation in permeability generates a heterogeneous seepage field in the local zone. The heterogeneous permeability may increase the reservoir impedance and shorten the lifetime of an EGS [12]. Therefore, in the process of heat extraction in HDR, the permeability enhancement and variation significantly affect the exploitation performance [32]. Unfortunately, most of the numerical models mentioned above ignore the dynamic matrix permeability variation in the whole heat extraction process. Only the variation of fracture permeability is considered in the seepage field. In rare researches [9], the matrix permeability variation is described by stress field, in which the thermal stress is induced by thermal unloading. Then, the impact of thermal unloading on the rock permeability is indirectly described. The stress–permeability model is developed based on some assumption. For example, the rock is treated as a homogeneous material. However, one of the critical reasons for the matrix permeability enhancement induced by thermal unloading is the inhomogeneity of materials in rock [1]. The current models cannot consider the key factor. Thus, it is necessary to develop a direct relationship between the thermal unloading and the matrix permeability variation in the coupling numerical model. However, to our knowledge, there is no work reported about the relationship in any numerical models. To further discuss the thermal-seepage-stress coupling field, the matrix permeability variation induced by thermal unloading should be considered in the numerical model. Then, a more reliable numerical model can be employed to study the geothermal exploitation performance.

This study develops a thermal–hydraulic–mechanical coupled three–dimensional model in COMSOL software, where the matrix permeability evolution induced by thermal unloading is emphasized. Unlike the traditional method, the matrix permeability enhancement is directly expressed by the thermal unloading, and the relationship between the two physical parameters is established according to the

previous experiment conducted by Cheng [33]. Then, the accuracy and reliability of the numerical model is validated by an existing analytical solution and a field measurement. Thereafter, the effect of the fracture number on geothermal exploration is discussed in the EGS. Generally, this work should help to analyze the heat exchange performance when multiple fractures are designed in an EGS.

2. Relationship between the matrix permeability enhancement and thermal unloading of rock

When a cryogenic fluid is injected into HDR, the abrupt change in the temperature of the rock surface leads to tensile stress, which can lead to rock damage. Certainly, a variation in the mechanical properties occurs to some extent. The permeability, which may change by more than one order of magnitude [28], should be considered in the process of heat extraction. To investigate the effect of thermal unloading on permeability enhancement, a series of experiments were conducted by Cheng [33]. The experiments were performed at a confining pressure of 7 MPa and a pore pressure of 3 MPa. The initial permeability of the specimen at room temperature was 0.0068 mD. In the process of heat treatment, the specimens were slowly heated to high temperature at a rate of 5 °C/h. Six high temperatures were considered: 100 °C, 200 °C, 300 °C, 400 °C, 500 °C and 600 °C. Then, the specimens were quickly cooled by cryogenic water at temperatures of 20 °C, 60 °C and 100 °C. The volume ratio of the cooling water to the specimen was 1000. After a sufficient cooling time, the rock temperature was regarded as equal to the temperature of the corresponding cooling water. The experimental results are shown in Table 1.

The experiments involved thermal loading and unloading. When the specimen was heated at high temperature, damage occurred due to the expansion of the particles. However, when the specimen was cooled quickly, the particles contracted, resulting in tensile damage. Compared to that induced by thermal loading, the permeability enhancement by thermal unloading is far greater [34]. Therefore, the role of heat treatment with a very slow rate in permeability enhancement is ignored, and the initial permeability before heat treatment is considered as the rock permeability under the high temperature conditions. Based on this assumption, the permeability enhancement induced by the temperature difference between the heated rock and the cryogenic water (ΔT) is studied. The parameter R is defined as the ratio of the permeability after water cooling (kc) to the initial permeability (ki). Combined with the experimental results (Table 1), a relationship between R and ΔT is obtained (as shown in Fig. 1). The matrix permeability enhancement is directly expressed by the thermal unloading, and the relationship between the two physical parameters is established according to the experiments. The curve is fitted with an exponential function with a correlation coefficient of 0.85. The expression is written as:

$$R = k_c / k_i = e^{0.0045\Delta T} \tag{1}$$

Table 1
Permeability of granite after thermal unloading [33].

Rock temperature (°C)	Rock permeability after cooling treatment (mD)		
	Cooling water at 20 °C	Cooling water at 60 °C	Cooling water at 100 °C
100	0.0088	0.0083	/
200	0.0137	0.0099	0.0115
300	0.0240	0.0202	0.0226
400	0.0628	0.0387	0.0484
500	0.1670	0.1106	0.1671
600	0.7231	0.6487	0.7068

3. Mathematical description of the THM model

3.1. Model assumptions

Heat extraction in an EGS is a complex process that involves THM coupling interactions. To develop a numerical model, the following assumptions are adopted to describe the processes of fluid seepage, heat transfer and rock deformation [7–18].

(1) The EGS reservoir is simplified to be consisted of a continuous rock matrix and discrete artificial fractures. The porous matrix is assumed as a homogenous and isotropic material, except the permeability.
(2) Under reservoir and operating conditions, water in the pores and fractures is assumed to be in the state of liquid.
(3) The reservoir is assumed to be fully saturated with water. The fluid flow in the rock matrix and fractures is described by Darcy's law and cubic law, respectively.
(4) Local thermal equilibrium is assumed between the solid rock and the fluid. Then the temperatures of the rock and fluid are equal at any point. The heat transfer process is described by Fourier's law.
(5) It is assumed that only the influence of temperature on the matrix permeability is considered. The effect of other factors is ignored. When the cryogenic fluid is injected into HDR, the matrix permeability enhancement is considered as a result of the abrupt change in the temperature of the rock surface. The relationship between the matrix permeability and the temperature decrease is shown in Fig. 1. The matrix permeability is modified by Eq. (1).
(6) The chemical reaction is not considered in the coupling process.

3.2. Governing equations

Based on the assumptions expressed above, the governing equations of the THM model during heat extraction are as follows:

3.2.1. Mechanical deformation equations

The HDR is a type of rock with high strength. In the numerical model, the reservoir rock is treated as an elastic material during heat extraction. The mechanical deformation of a rock block is induced by in situ stress, thermal stress and fluid pressure. The total strain can be defined as [35].

$$\varepsilon_{kl} = \frac{1}{2G}\sigma_{kl} - \left(\frac{1}{6G} - \frac{1}{9K}\right)\sigma_{dd}\delta_{kl} + \frac{\alpha p}{3K}\delta_{kl} + \frac{\alpha_T T}{3}\delta_{kl} \tag{2}$$

where ε_{kl} is the strain component; $G = E/(2+2\nu)$ is the shear modulus, Pa; $K = E/3(1\text{-}2\nu)$ is the bulk modulus, Pa; E is the Young's modulus, Pa; ν is Poisson's ratio; σ_{kl} is the stress component, Pa; σ_{dd} is the normal stress component, Pa; δ_{kl} is the Kronecker symbol; α is the Biot coefficient; p is the water pressure; and α_T is the thermal expansion coefficient, $1/K$.

Combined with the equilibrium equation and the strain–deformation relation equation, the governing equation of the stress field is written as

$$Gu_{k,ll} + \frac{G}{1-2\nu}u_{l,lk} - \alpha p_{,k} - K\alpha_T T_{,k} + f_k = 0 \tag{3}$$

where f_k is the volume force component, N.

The deformation of the embedded fracture is written as [36].

$$u_n = \frac{\sigma_n^{'}}{K_n^*} \quad \sigma_n^{'} = \sigma_n - \alpha p \tag{4}$$

$$u_s = \frac{\sigma_s^{'}}{K_s^*} \quad \sigma_s^{'} = \sigma_s \tag{5}$$

where u is the normal displacement, m; K^* is the stiffness of the fracture, Pa/m; and σ and σ' are the total stress and the effective stress acting on the fracture, respectively, Pa. The subscripts n and s represent the normal and tangential directions to the fracture surface, respectively.

3.2.2. Fluid flow equations

The fluid flow in the rock matrix and the fracture is described by the mass conservation law [37], in which the effect of the rock matrix deformation and the fractures are considered.

$$S\frac{\partial p}{\partial t} + \nabla \cdot q = -\alpha \frac{\partial \varepsilon_v}{\partial t} - Q_f \tag{6}$$

$$d_f S_f \frac{\partial p}{\partial t} + \nabla_\tau \cdot \left(d_f q_f\right) = -d_f \alpha \frac{\partial \varepsilon_v}{\partial t} + d_f Q_f \tag{7}$$

where S is the storage coefficient of the rock matrix, Pa^{-1}; t is the time, s; q is the Darcy velocity, m/s; d_f is the fracture aperture, m; S_f is the storage coefficient of the fracture, Pa^{-1}; q_f is the Darcy velocity in the fracture, m/s; ε_v is the volume strain; and Q_f is the mass transfer between the rock matrix and the fracture, 1/s.

According to Darcy's law, q and q_f are described by the following equations

$$q = -\frac{k}{\mu_f}\nabla \cdot (p + \rho_w gz) \tag{8}$$

$$q_f = -\frac{k_f}{\mu_f}\nabla_\tau \cdot (p + \rho_w gz) \tag{9}$$

where k is the matrix permeability, m^2. k is related to the temperature change and is calculated by Eq. (1). k_f is the fracture permeability, m^2. k_f is determined by the fracture width and is calculated by $12/d_f^2$. μ_f is the dynamic fluid viscosity, Pa·s; ρ_w is the fluid density, kg/m³; g is the gravitational acceleration, m/s²; and z is the unit vector in the vertical direction.

The dynamic fluid viscosity μ_f is determined by the temperature, which is written as:

$$\mu_f = \begin{cases} 1.3799 - 0.0212T + 1.3604 \times 10^{-4}T^2 - 4.6454 \times 10^{-7}T^3 + 8.9043 \times 10^{-10}T^4 \\ -9.0791 \times 10^{-13}T^5 + 3.8457 \times 10^{-16}T^6 \quad 273.15K \leq T < 413.15K \\ 0.004 - 2.1075 \times 10^{-5}T + 3.8577 \times 10^{-8}T^2 - 2.3973 \times 10^{-11}T^3 \quad 413.15K \leq T \leq 573.15K \end{cases} \tag{10}$$

3.2.3. Heat transportation equations

Between the rock matrix and the injected fluid, the local thermal equilibrium is adopted to describe heat exchange. Then, in any position, the temperatures of the solid and the liquid is the same as those in the EGS. The energy conservation equations in the matrix and the fracture are written as [17].

$$(\rho c_p)_m \frac{\partial T}{\partial t} + \nabla \cdot (\rho_w c_{p,w} qT) - \nabla \cdot (\lambda_m \nabla T) + K\alpha_T T\frac{\partial \varepsilon_V}{\partial t} = -Q_{f,E} \tag{11}$$

$$d_f (\rho c_p)_f \frac{\partial T}{\partial t} + \nabla \cdot (d_f \rho_w c_{p,w} q_f T) - \nabla_\tau \cdot (d_f \lambda_f \nabla T) + d_f K\alpha_T T\frac{\partial \varepsilon_V}{\partial t} = d_f Q_{f,E} \tag{12}$$

where T is the temperature, K; $c_{p,w}$ is the heat capacity of the fluid, J/
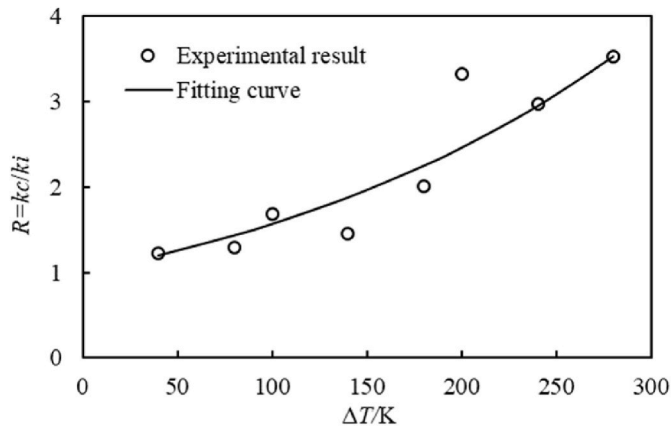
Fig. 1. Variation in R due to water cooling.

(kg·K); $Q_{f,E}$ is the heat exchange between the rock matrix and the fracture, W/m³; $(\rho c_p)_m$ and $(\rho c_p)_f$ are the effective volumetric heat capacities of the matrix and the fracture, respectively, J/(m³·K); and λ_m and λ_f are the effective thermal conductivities of the matrix and the fracture, respectively, W/(m·K).

$$\left(\rho c_p\right)_m = (1-\varphi)\rho_s c_{p,s} + \varphi \rho_w c_{p,w} \tag{13}$$

$$\left(\rho c_p\right)_f = \left(1-\varphi_f\right)\rho_s c_{p,s} + \varphi_f \rho_w c_{p,w} \tag{14}$$

$$\lambda_m = (1-\varphi)\lambda_s + \varphi\lambda_w \tag{15}$$

$$\lambda_f = \left(1-\varphi_f\right)\lambda_s + \varphi_f\lambda_w \tag{16}$$

where φ and φ_f are the porosities of the matrix and the fracture, respectively; ρ_s is the solid density, (kg/m³); $c_{p,s}$ is the solid heat capacity, J/(kg·K); and λ_s and λ_w are the thermal conductivities of the solid and the fluid, respectively, W/(m·K).

The heat capacity ($c_{p,w}$), the thermal conductivities (λ_w) and the density (ρ_w) are related to the temperature, which are written as follows:

$$c_{p,w} = 12010 - 80.4T + 0.3T^2 - 5.4 \times 10^{-4}T^3 + 3.6 \times 10^{-7}T^4 \quad 273.15K$$
$$\leq T \leq 573.15K \tag{17}$$

$$\lambda_w = 7.9754 \times 10^{-9}T^3 - 1.5837 \times 10^{-5}T^2 + 0.0089T - 0.8691 \quad 273.15K$$
$$\leq T \leq 573.15K \tag{18}$$

$$\rho_w = 838.4661 + 1.4005T - 3 \times 10^{-3}T^2 - 3.7182 \times 10^{-7}T^3 \quad 273.15K \leq T$$
$$\leq 573.15K \tag{19}$$

3.3. Coupling relationships

The numerical simulation involves the complicated coupled THM process, as shown in Fig. 2. The interaction between different processes is expressed as follows:

1) Relationship between the stress field and the seepage field. With fluid injection, the pore pressure (p in Eqs. (2)–(4)) in the EGS is disturbed, which affects the effective stress (σ' in Eq. (2) and Eq. (4)) acting on the rock. Rock deformation (ε_v in Eqs. (6) and (7)) results in changes in the pore pressure (p in Eqs. (6) and (7)) and fracture permeability (k_f in Eq. (9)).
2) Relationship between the stress field and the temperature field. The variation in the reservoir temperature (T in Eqs. (2) and (3)) induces
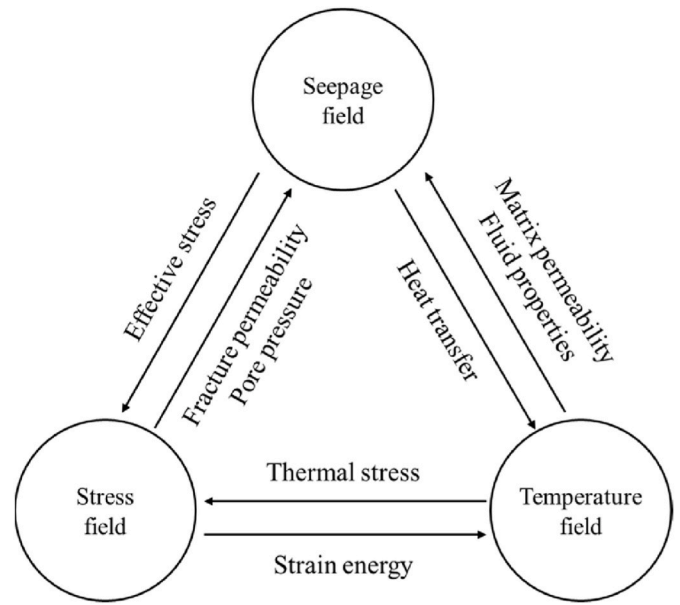

Fig. 2. Coupled THM relationship.

thermal stress, which can disturb the stress field (σ in Eq. (2)) and displacement field (u in Eq. (3)). Rock deformation (ε_v in Eqs. (11) and (12)) generates strain energy acting as a type of heat source in the heat transfer process (T in Eqs. (11) and (12)).
3) Relationship between the seepage field and the temperature field. The properties of the fluid (μ_f in Eqs. (8) and (9); $c_{p,w}$, λ_w and ρ_w in Eqs. (11) and (12)) and the matrix permeability after cooling (k_c in Eq. (1)) are affected by the temperature variation (T in Eqs. (1), (10) and (16)–(18)). The fluid flow (q in Eqs. (11) and (12)) leads to heat exchange (T in Eqs. (11) and (12)) between the cryogenic fluid and the rock at high temperatures, which affects the temperature distribution.

The coupled THM process, as well as the governing equations is realized in the COMSOL Multiphysics solver.

4. Validation of the coupled THM model

To validate the coupled THM model developed in the paper, the existing analytical solution and field measurement are adopted as
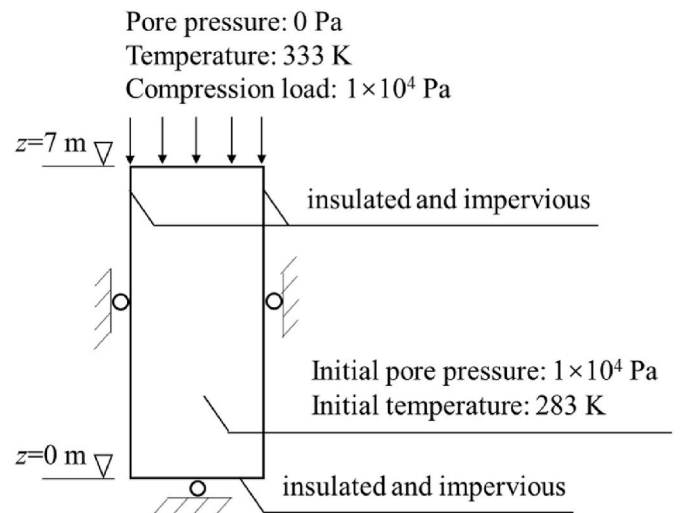

Fig. 3. Description of the thermoelastic consolidation model.

simulation examples.

4.1. Validation of the analytical solution

The thermoelastic consolidation problem of a saturated soil column is utilized to demonstrate the accuracy of the coupled THM model [10]. Based on the finite Fourier transform and its inverse transform, Bai [38] deduced the analytical solutions of the thermal elastic consolidation model under nonisothermal conditions. The one-dimensional model is described in Fig. 3. In the numerical model, the height of the soil column is 7 m. The initial pore pressure and temperature are set to 1×10^4 Pa and 283 K, respectively. At the top surface, the compression load is 1×10^4 Pa. In addition, a pore pressure of 0 Pa and a temperature of 333 K are also applied. The other three boundaries are considered thermally insulated and impervious, and the displacement is constrained in the normal direction. The numerical parameters are listed in Table 2.

The comparison between the analytical solution and the numerical results is shown in Fig. 4. The results include the temperature, pore pressure and displacement at different positions. The results obtained from the numerical model are identical to the analytical solution. Thus, the accuracy of the coupled THM model is verified.

4.2. Validation of the field measurement

Field measurements obtained from the Fenton Hill Phase I site were employed to validate the numerical model developed in the study. A conceptual description of the EGS is shown in Fig. 5 [39]. The diameter of the artificial fracture was 120 m. The injection well was located at a depth of 2750 m and connected 25 m from the bottom of the fracture. The production well was located at a depth of 2670 m and connected 15 m from the top of the fracture. The heat extraction performance of HDR was evaluated with 75 days of closed-loop operation [39]. At the location of the injection well, the rock temperature was 185 °C. The geothermal gradient was 100 °C/km under a depth of 2300 m. During the 75-day circulation test, the injection rate in the first 25 days was 7.5 kg/s. Then, the rate gradually increased to 15 kg/s between days 26 and 36, and remained constant in the following 36 days (Fig. 6a). Because of heat exchange between the injection water and borehole wall, the water temperature at the entry point was variable. The injection temperature variation with time is show in Fig. 6b [40]. During the process, the pressure at the extraction point ranged from 25 MPa to 26.5 MPa. In the numerical model, a constant pressure of 25 MPa was employed for the production well. In addition, the minimum horizontal stress, the maximum horizontal stress and the vertical stress were 37 MPa, 53 MPa and 74 MPa, respectively [15,39]. The rock was treated as linear elastic, homogeneous and isotropic. Some of the properties of the reservoir rock are shown Table 3 [40].

The measured injection pressure (at a depth of 2750 m) and production temperature (at a depth of 2670 m) are utilized to validate the reliability of the developed numerical model. Before heat extraction in the field, an abundant of fluid had been injected into the reservoir to form a hydraulic fracture. During the fracturing process, the reservoir had been cooled to a certain degree. As shown in Fig. 7b, the production temperature decreased once the cryogenic fluid was injected into the reservoir. However, in the numerical simulation, it takes a period time for the injected fluid to reach the production well. Hence, the extraction

temperature decreases slowly in the early stage. In the numerical results, after fluid injection with a period time, the extraction temperature decreases to 173 °C which is equal to the initial extraction temperature in the field measurement. To better compare the numerical results and the experimental results, we choose the time when the extraction temperature is 173 °C as the initial injection time. Within the injection of 75 days, the injection pressure and production temperature curves obtained from the numerical simulation and the field measurement are shown in Fig. 7. The variation trends of the curves are similar. In general, the simulation results exhibit an acceptable agreement within the field measurements to a certain degree. Therefore, the coupled THM model is reliable for predicting the heat extraction performance in an EGS.

5. Multifracture EGS model

5.1. Description of the conceptual model

A schematic of the conceptual numerical model is illustrated in Fig. 8. The reservoir is located at a depth of 4500–5300 m with the dimensions of 500 m × 500 m × 400 m. The EGS is in the centre of the reservoir with the dimensions of 300 m × 300 m × 200 m (Fig. 8a). The horizontal wells consist of one injection well and one production well and are 400 m below the top of the reservoir. The well length, well diameter and well spacing are 300 m, 280 m and 0.2 m, respectively. In the EGS, vertical artificial fractures are designed to connect the injection well and the production well. To analyze the effect of the fracture spacing (Sp) and number (N) on the heat extraction performance, different numerical cases are designed in the study. As shown in Fig. 8b, four types of fracture numbers are employed, namely, $N = 2$ ($Sp = 100$ m), $N = 3$ ($Sp = 75$ m), $N = 4$ ($Sp = 60$ m), and $N = 5$ ($Sp = 50$ m). The relevant physical parameters are listed in Table 4.

5.2. Initial and boundary conditions

The initial and boundary conditions of the THM model are listed as follows:

(1) Stress field. The vertical stress (σ_z) applied to the top surface is based on the overlying rock weight. At a depth of 4500 m, σ_z is set to 122 MPa. The lateral pressure coefficients used to calculate the horizontal stresses are 0.8 and 0.7, and the maximum horizontal stress (σ_y) and the minimum horizontal (σ_x) stress are 98 MPa and 85 MPa, respectively.
(2) Seepage field. The mass flow rate of the injection well maintains a constant value of 30 kg/s. The production pressure is fixed at 30 MPa. The initial pressure of the reservoir is 40 MPa, and the pressure gradient is ignored. The surrounding boundaries are permeable, with a constant pressure of 40 MPa. The upper and lower boundaries are impermeable.
(3) Temperature field. The initial temperature (T_0) is 573.15 K, and the temperature gradient is ignored in the model. The injection temperature (T_{inj}) of the fluid is fixed at 303.15 K. The surrounding boundaries are set to 573.15 K, and the upper and lower boundaries are thermal insulation.

6. Results and discussion

6.1. Effect of matrix permeability evolution on heat extraction performance

6.1.1. Temperature variation in the intersection point of fracture and production well

To analyze the effect of the matrix permeability evolution on the heat extraction performance, the temperature variation of the production well is discussed. The numerical model with two fractures ($N = 2$) is taken as an example. Herein, the point which is in the intersection point

Table 2
Parameters of the thermoelastic consolidation model.

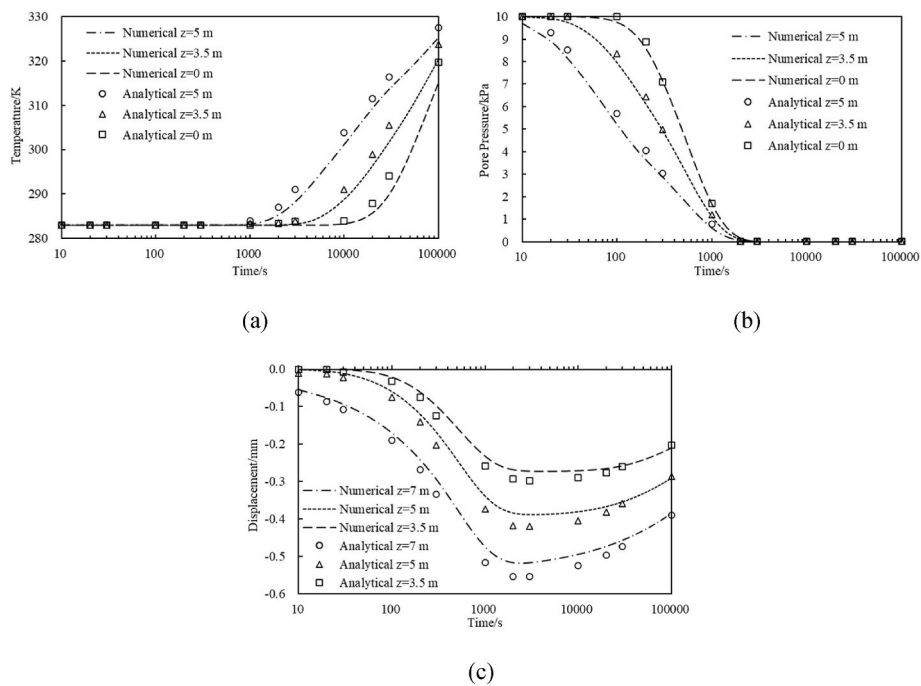| Parameter	Value	Parameter	Value
Density of soil	2000 [kg/m³]	Storage coefficient	2e-9 [1/Pa]
Elastic modulus	6e7 [Pa]	Thermal conductivity	30 [W/(m·K)]
Poisson's ratio	0.4	Heat capacity	100 [J/(kg·K)]
Biot coefficient	1	Expansion coefficient	3e-7 [1/K]
Porosity	0.2	Hydraulic conductivity	4e-6 [m/s]

Fig. 4. Variation in results with time at different positions: (a) temperature; (b) pore pressure; and (c) displacement.
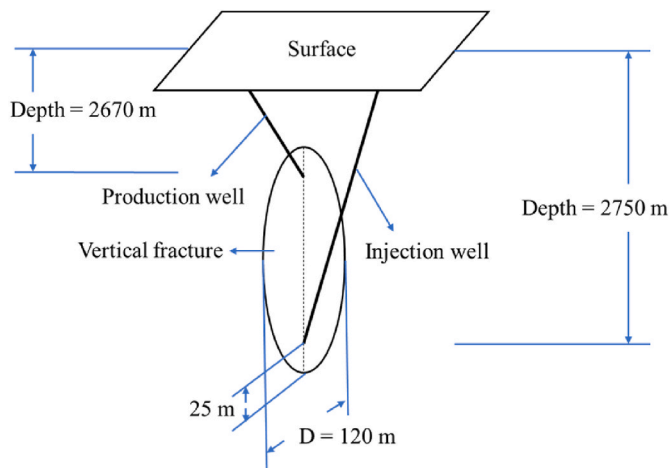

Fig. 5. Conceptual arrangement of the reservoir.

of fracture and production well is selected to discuss the temperature variation. Noted that the numerical model that considers the matrix permeability evolution is referred to as the modified model, and the

numerical model that does not consider the matrix permeability evolution is referred to as the traditional model. As shown in Fig. 9, regardless of whether the matrix permeability evolution is considered in the numerical model, the variation trends of the curves are similar. In the early injection stage (0–1000 days), the temperature difference can be ignored. With more cryogenic fluid arrives at the production well, the decline rates of the temperature are different. The temperature obtained from the modified model is lower than the traditional temperature. The maximum temperature difference can reach 20 K after 2000 days. Due to the limited heat exchange area in the fracture, the recovery rate decreases, and the temperature variation becomes gentle for the two models. After 6000 days, the values of the temperature difference can be ignored. Finally, the temperature decreases from 573.15 K to 370 K after water injection of 10000 days for the two models. Thus, if the matrix

Table 3
Properties of the reservoir rock.

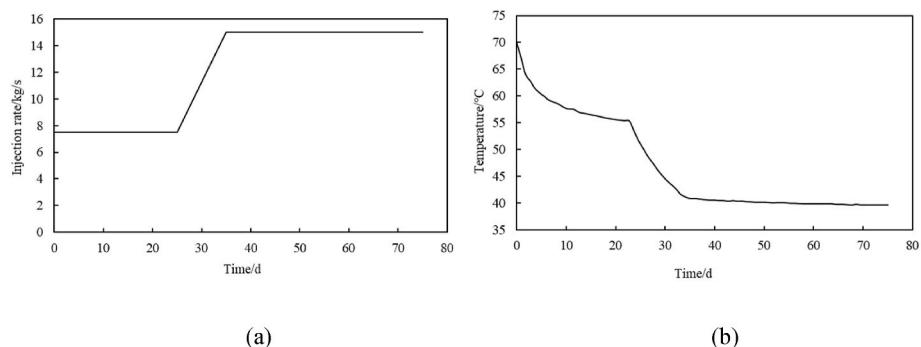| Parameter	Value	Parameter	Value
Density	2700 [kg/m^3]	Thermal conductivity	2.9 [W/(m·K)]
Elastic modulus	25e9 [Pa]	Heat capacity	900 [J/(kg·K)]
Poisson's ratio	0.25	Expansion coefficient	3e-6 [1/K]
Fracture aperture	1e-5 [m]	Permeability	1e-18 [m^2]

Fig. 6. Boundary conditions at the fracture injection point: (a) water injection rate and (b) water temperature.
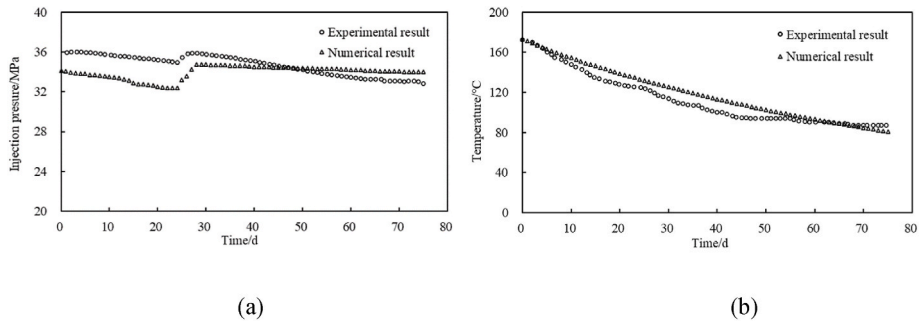
Fig. 7. Comparison between the field measurement and numerical simulation: (a) injection pressure at a depth of 2750 m and (b) extraction temperature at a depth of 2670 m.
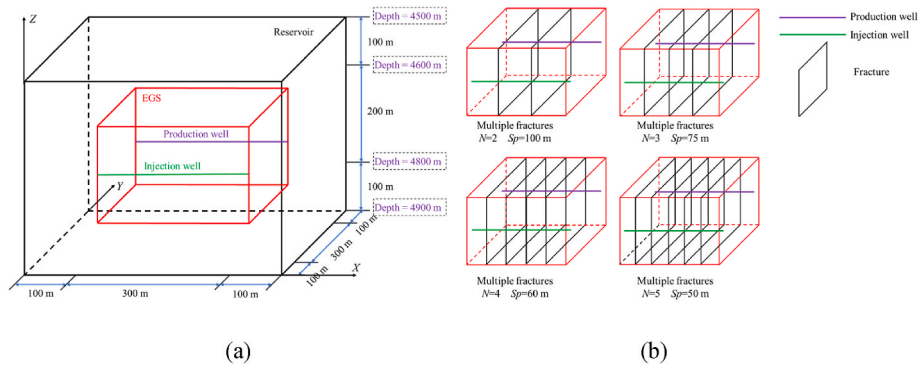

Fig. 8. Conceptual model of the EGS: (a) schematic diagram of the reservoir and (b) EGS design for different cases.

Table 4
Reservoir physical properties.

| Parameter	Value	Parameter	Value
Matrix density	2700 [kg/m^3]	Fracture density	2700 [kg/m^3]
Matrix porosity	0.1	Fracture porosity	1
Matrix elastic modulus	25e9 [Pa]	Fracture stiffness	2e12 [Pa/m]
Matrix Poisson's ratio	0.2	Fracture initial aperture	5e-4 [m]
Matrix permeability	1e-17 [m^2]	Fracture heat capacity	850 [J/(kg·K)]
Matrix heat capacity	1000 [J/(kg·K)]	Fracture thermal conductivity	2 [W/(m·K)]
Matrix thermal conductivity	2.5 [W/(m·K)]	Expansion coefficient	5e-6 [1/K]
Fluid compressibility	3e-8 [1/Pa]	Biot coefficient	1
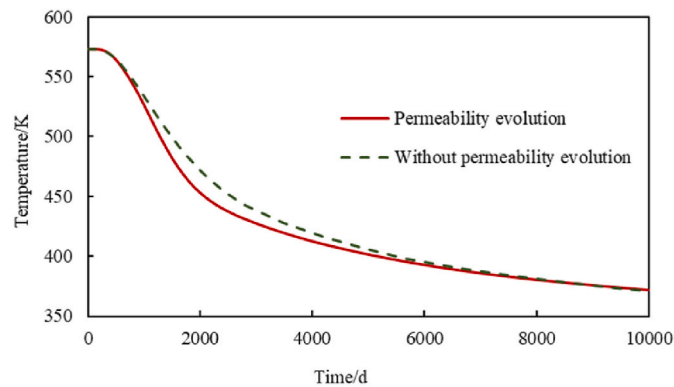
Fig. 9. Temperature variation curves with time at the point which is located at the intersection point of fracture and production well.

permeability evolution is ignored in the numerical model, the production temperature is overestimated from 1000 to 6000 days.

6.1.2. THM coupling field

The heat exchange in the EGS involves complex THM coupling process. The effect of the matrix permeability evolution on coupling physical field, namely temperature field, seepage field and stress field, is discussed. Fig. 10 shows the distribution of the physical variates after the injection of 2000 days. The production pressure (30 MPa) is lower than the initial pressure (40 MPa). During the injection process, the pressure in the fracture is lower than the pore pressure in the matrix. Due to the pressure gradient, fluid is transported from the matrix into the fracture. As the rock around the fracture is cooled by cryogenic water, the matrix permeability becomes higher in the modified model. Then, compared with the traditional model, more water flow from the matrix into the fracture. Fig. 10a shows the pressure distribution in the fracture. When the matrix permeability evolution is considered in the model, the pressure and the pressure gradient are slightly higher. For example, the highest values of the pressure are 32 MPa (the modified model) and 31 MPa (the traditional model), respectively. The fracture width difference for the two models can be ignored. However, the values of the fluid velocity in the fracture are different. Along the straight line connecting the two wells, the average velocity in the modified model is 2.5 times that of the traditional model. Hence, the heat extraction is quicker in the modified model. Under the influence of the seepage condition, the temperature decreases quickly along the fracture length direction (Fig. 10b). Additionally, the variation in the seepage field explains why the temperature obtained from the modified model is lower than that obtained from the traditional model from 1000 to 6000 days (Fig. 9). Based on the relationship between the matrix permeability and the temperature decrease (Fig. 1), the permeability variation of the fracture surface is shown in Fig. 10c. The variable permeability can be up to 3.5 times the initial permeability. According to the coupling relationship, the stress evolution is affected by the pressure and the

(a)

(b)

(c)

(d)
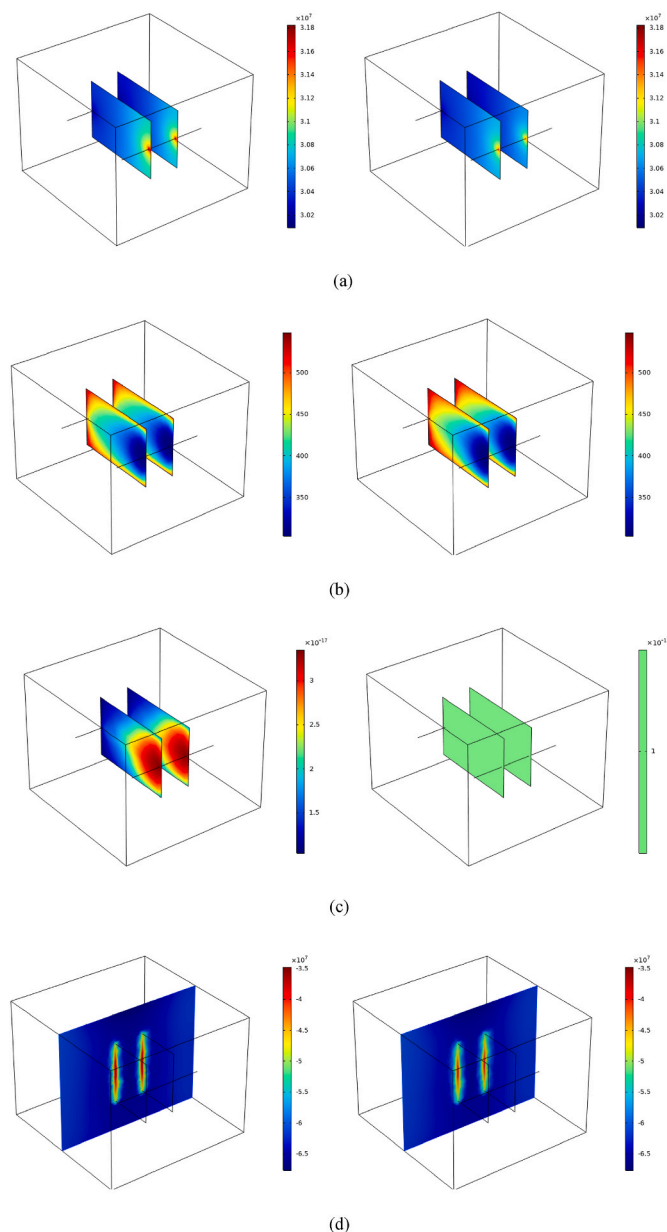
Fig. 10. Distribution of the physical variates after 2000 days: (a) fluid pressure in the fracture; (b) temperature in the fracture surface; (c) matrix permeability of the fracture surface; and (d) effective stress along the direction which is perpendicular to the fracture. Note that the results of the left column consider the matrix permeability evolution, while the right column does not consider the matrix permeability evolution.

temperature variation. Hence, with the injection of cryogenic water, the stress field is obviously disturbed around the fractures. The effective stress (negative represents compressive stress) along the direction which is perpendicular to the fracture is shown in Fig. 10d. The pressure around the fractures is smaller than 40 MPa. Smaller pressure leads to higher compressive stress. However, thermal unloading generates tension stress, and the effective stress around the fracture is smaller than other region. Thus, it can be concluded that compared with the pressure, the temperature variation plays an important role in the stress field. When the matrix permeability evolution is considered in the model, the stress distribution is similar for the two models. As analyzed above, the heat exchange process in the fracture exhibits a quicker rate in the modified model. The more quickly the temperature drops in the rock, the greater the tensile stress is generated. As shown in Fig. 10d,

compared to the traditional model, the effective stress around the fracture is smaller in the modified model. Generally, with the injection of cryogenic water, the temperature field, the seepage field and the stress field are all disturbed. During the coupling process, the effect of the matrix permeability evolution induced by thermal unloading can affect the coupling field to a certain extent.

6.2. Effect of fracture number on heat extraction performance

6.2.1. Temperature evolution in the production well

The temperature distribution along the production well is shown in Fig. 11. Due to the existence of the artificial fractures, the temperature distribution presents a wavelike change along the production well rather than an approximate straight line. The troughs are located at the fracture, and the peaks are located between the fractures or at the EGS boundary. In the early stage, the cooling area is mainly located around the fractures. More fractures are advantageous for expanding the cooling range along the production well (Fig. 11a). After 10000 days, the temperatures at the curve troughs are similar for the four numerical cases. However, more wells result in a lower temperature at the curve peaks (except for the EGS boundary).

The fracture and matrix are the two seepage channels for the fluid in geothermal exploitation. To discuss the effect of the fracture number on the temperature in the production well during the whole heat exchange process, three points are selected (Fig. 12), namely, the point located at the intersection of the fracture and the well (IF), the point located between two fractures (BF), and the point located between an EGS boundary and a fracture (OF).

As shown in Fig. 13, the temperatures of both the fracture (IF) and the matrix (BF and OF) are greatly affected by the fracture number. The fracture permeability is greater than the matrix permeability. When the fracture number increases from 2 to 5 in the EGS, the flow rate of the water decreases in a single fracture. This difference leads to a smaller amount of heat exchange between the cryogenic fluid and the rock at high temperatures. Therefore, the temperature at the IF point decreases more slowly for the EGS with more fractures (Fig. 13a). For example, after 2000 days, the temperature drop values are 61 K ($N = 5$), 87 K ($N = 4$), 103 K ($N = 3$) and 120 K ($N = 2$). At the IF point, the temperature difference (ΔT) between the case with 5 wells and the other three cases exhibits the following characteristics: (1) In the first stage, the efficiency of heat exchange is high, and ΔT keeps increasing once the injected water arrives at the production well; (2) In the second stage, the efficiency of heat exchange is low, especially for the EGS with fewer wells. Then, ΔT begins to decrease after the maximum value is reached. Finally, at the IF point, the values of T are nearly the same after 10000 days for the four numerical cases.

Unlike the temperature variation at the IF point, the temperature at the BF point or OF point exhibits different variations. Due to the small pressure difference between the two wells, the flow rate of the fluid in the matrix is affected by the permeability. Thus, the permeability evolution induced by thermal unloading is very important. Artificial fractures are the main seepage channels for fluids. The thermal unloading of the rock in the EGS is mostly induced by the cryogenic fluid in the fracture. When there are more fractures in the EGS, the fracture distance is shorter. Under the condition of heat exchange between the fracture and the rock surface, the cooling degree of the matrix is greater. As shown in Fig. 14, the effect of the fracture number on the rock cooling degree is especially exhibited in the fracture length direction. Given the relationship between the matrix permeability and thermal unloading, an EGS with more fractures is advantageous for the matrix permeability enhancement, resulting in a larger amount of water being transported from the injection well to the production well. During the process, the efficiency of heat exchange is higher. Hence, the temperature at the BF point or the OF point is lower for the EGS with more fractures, which is different from point IF (Fig. 13b). For the points in the matrix, the temperature at the BF point decreases more rapidly than that at the OF
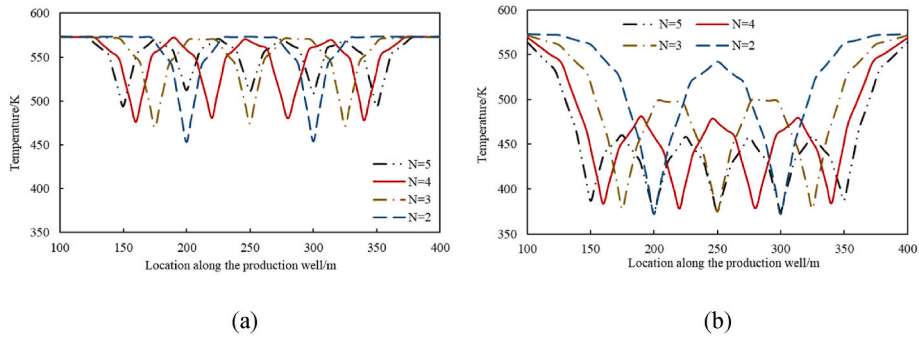
(a)   (b)

Fig. 11. Effect of fracture number on the temperature distribution along the production well: (a) after 2000 days and (b) after 10000 days.
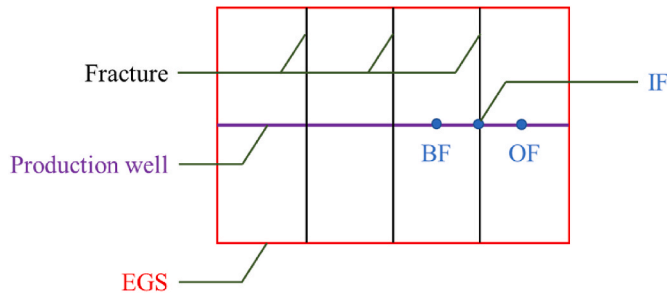

Fig. 12. Section view of the EGS (e.g., the EGS with four fractures).

point. This is mainly for two reasons: (1) compared with the BF point, the OF point is closer to the unstimulated reservoir, and (2) the degree of thermal unloading in the region between two fractures is greater than that in the region between an EGS boundary and a fracture, resulting in different seepage fields of the two regions. With more fractures in the EGS, the temperature difference between the BF point and the OF point ($\Delta T_{\mathrm{BF\text{-}OF}}$) is greater. For example, after 10000 days, the values of $\Delta T_{\mathrm{BF\text{-}OF}}$ are 62 K ($N = 5$), 55 K ($N = 4$), 44 K ($N = 3$) and 20 K ($N = 2$).

To evaluate geothermal exploration, the production temperature

(T_{out}) is an important index. T_{out} relates to the coupled field in the rock matrix and the fracture. Thereby, T_{out} is defined as

$$T_{out} = \frac{\sum u_f d_f T + \int_{\Omega} u T d\Omega}{\sum u_f d_f + \int_{\Omega} u d\Omega} \tag{20}$$

where u_f and u are the fluid velocities in the fracture and the matrix, respectively, m/s; Ω represents the wellbore.

According to the numerical results, $\sum u_f d_f$ is much greater than $\int_{\Omega} u d\Omega$. Compared with the matrix channel, the fracture channels play a major role in determining the variation in T_{out}. Thus, the effect of the fracture number on T_{out} is similar to that of the temperature at the IF point (Fig. 13a and c). Due to the different temperature variation characteristics in the matrix (e.g., T at the BF or OF point is higher with fewer fractures in the EGS), T_{out} decreases more quickly ($N = 5$ and 4) or slightly slower ($N = 3$ and 2) compared with the temperature at the IF point. For example, after 2000 days, the temperature drop values are 70 K ($N = 5$), 94 K ($N = 4$), 100 K ($N = 3$) and 118 K ($N = 2$). Through the above analysis, the artificial fractures can significantly improve heat exchange in the EGS. More importantly, for the same amount of injected water, an EGS with more fractures is prone to obtain a higher production temperature.
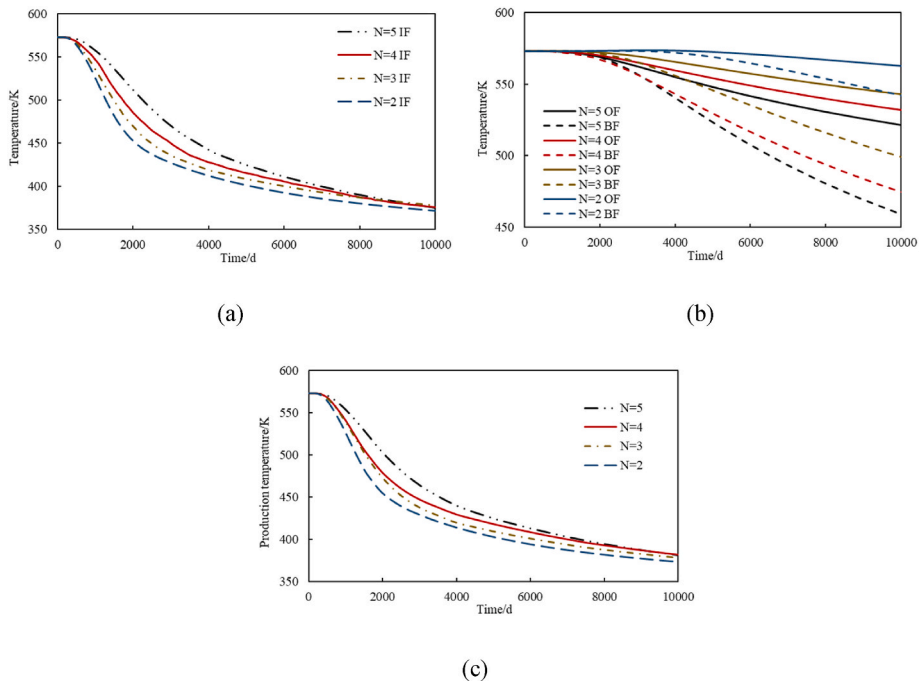

(a)   (b)

(c)

Fig. 13. Temperature variation curves with time at different locations of the production well: (a) IF and (b) BF and OF. (c) Production temperature of the production well.
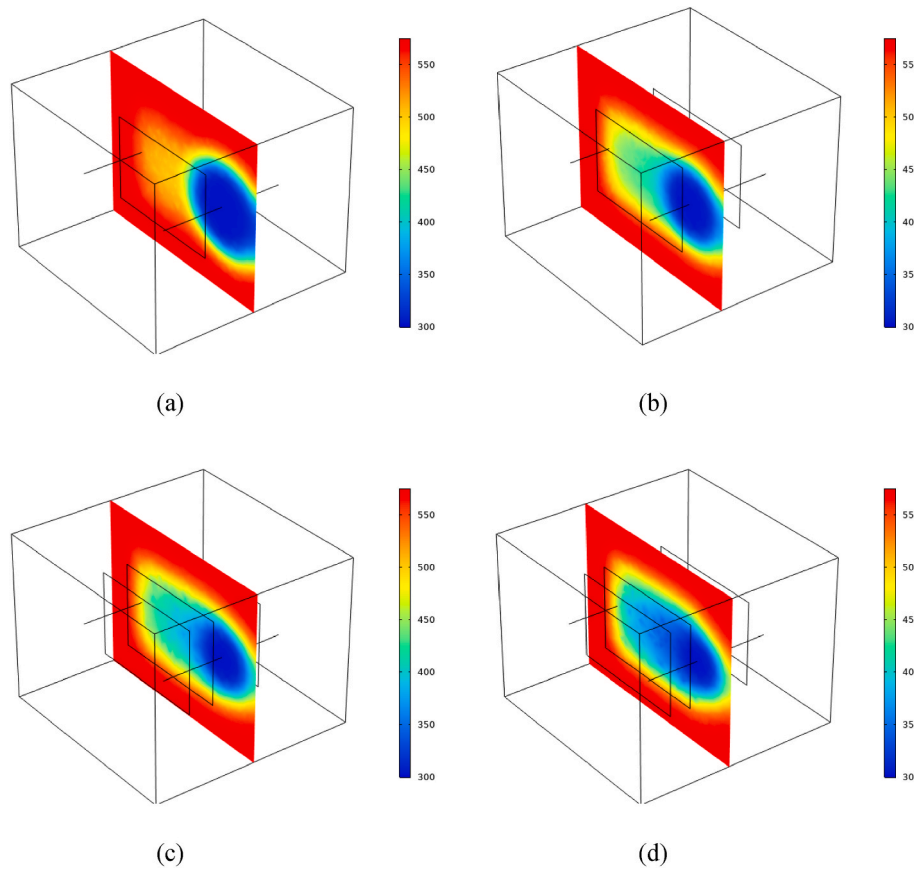
Fig. 14. Effect of fracture number on the temperature distribution in the section plane between two fractures after 10000 days: (a) N = 2; (b) N = 3; (c) N = 4 and (d) N = 5.

6.2.2. Temperature evolution in the EGS

The temporal and spatial evolution of the temperature in the *x-y* plane (at a depth of 4700 m) and *x-z* plane (*y* = 250 m) is shown in Fig. 15. In the EGS, as the cryogenic fluid is continuously injected into the reservoir, heat transportation occurs in the fracture and the rock matrix. In the fracture length and height directions, heat transportation is much faster in the fracture than in the matrix. However, the cooled rock affected by the fracture channel is limited to the narrow zone surrounding the fracture. On the other hand, the zones with low temperature in the rock matrix form slowly. Compared with the narrow zone affected by heat exchange in the fracture, the range of the cooled zone in the rock matrix is much wider. Due to the existence of the fractures, heat transportation in the rock matrix is categorized into two types: heat transportation (1) between fractures (region A) and (2) far from fractures (region B). As Fig. 15 shows, the cooling region between the fractures is greatly affected by the fracture number. For example, when the fracture number is two, the heat transportation rate in region A is similar to that in region B. When the fracture number increases to five, the cooling zone in region A forms much more quickly in the directions of the fracture height and length. In geothermal exploration, the ideal process is that heat exchange occurs at a wider range in the EGS. According to the analysis, the fracture number plays an important role in considering both the heat transportation and the cooling range in a geothermal exploration process.

To further discuss the temperature evolution in the EGS, the heat extraction ratio η is defined as the heat recovery divided by the total heat stored in the EGS:

$$\eta = \frac{\iiint\limits_{V_s} \rho_s c_{p,s} (T_0 - T) dV}{\iiint\limits_{V_s} \rho_s c_{p,s} (T_0 - T_{inj}) dV} \tag{21}$$

where V_S is the heat extraction zone in the EGS.

The effect of fracture number on the heat extraction ratio is shown in Fig. 16. According to Equation (17), η is affected by the temperature decrease in the fracture and in the matrix in the whole EGS, not just the production well. Fig. 15 displays the temperature distribution in the EGS after 10000 days. More fractures are beneficial for heat exchange in the fracture and region A. The total amounts of cryogenic fluid injected into the reservoir are equal for the four cases. When less water is transported from the injection well to the production well through the fracture channel, it is inevitable that more water flows in the matrix. Thus, the cooling zone, as well as the temperature decrease in region B, is larger when there are fewer fractures. Based on geothermal exploration in the matrix and in fracture, there is only a slight difference in the heat extraction ratios for the four numerical cases.

7. Summary and conclusions

In this paper, a conceptual EGS numerical model combining horizontal wells and multiple fractures is developed. The novel model considers the relationship between the matrix permeability enhancement and thermal unloading of rock. Then, the effect of fracture number on the heat extraction performance is analyzed. The conclusions are summarized as follows:

(1) At the intersection point of fracture and production well, the variation trends of the temperature curves obtained from the two models are similar. However, the decline rate is affected by the matrix permeability evolution. Within 1000–6000 days, the temperature obtained from the modified model is lower and the maximum temperature difference can reach 20 K. When
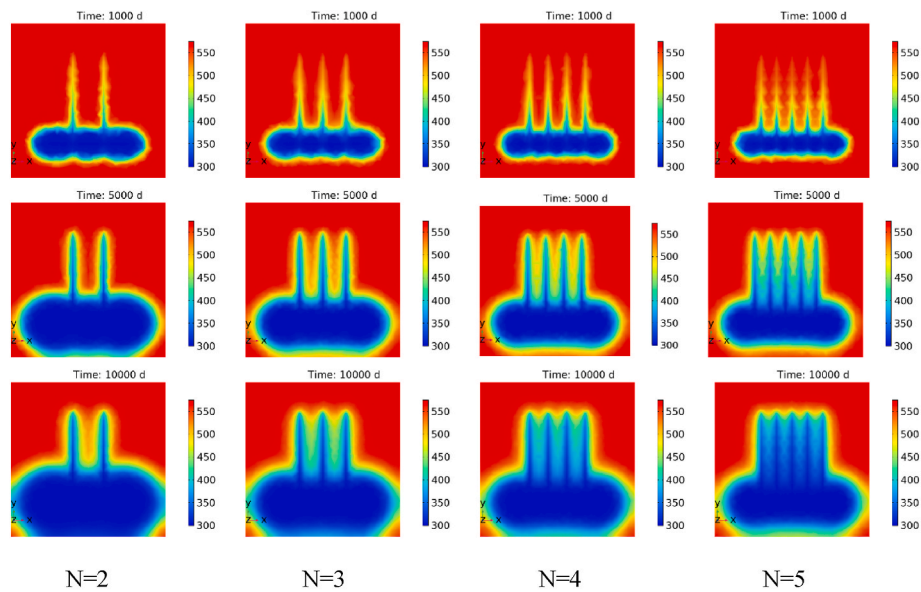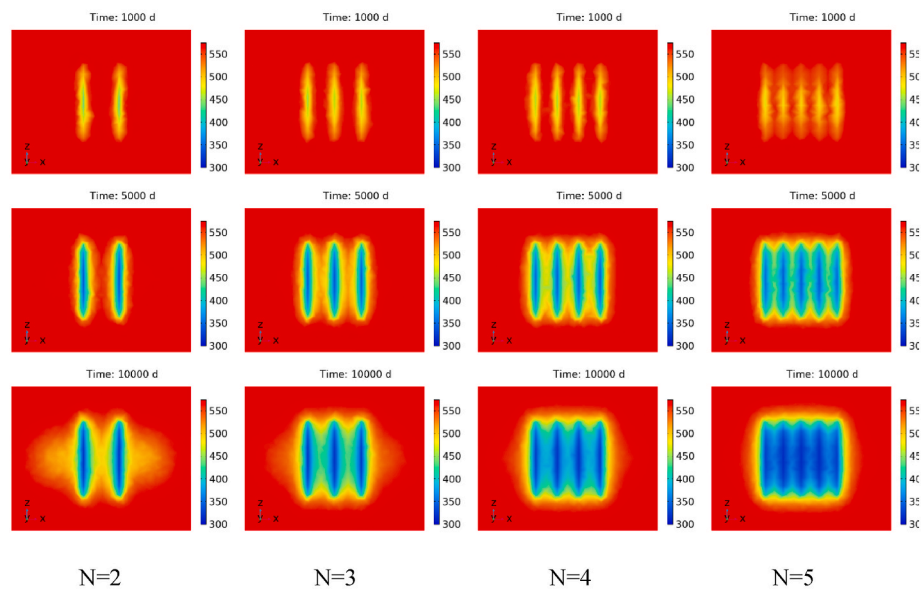
Fig. 15. Effect of fracture number on the temperature distribution: (a) in the *x-y* plane (at a depth of 4700 m) and (b) in the *x-z* plane (*y* = 250 m).

cryogenic water is injected into the reservoir, the coupling field is distributed. The effect of the matrix permeability evolution induced by thermal unloading can affect the coupling field to a certain extent.

(2) More fractures are advantageous for expanding the cooling range along the production well. The temperatures of both the fracture (IF) and the matrix (BF and OF) are greatly affected by the fracture number. The temperature at the IF point decreases more slowly for the EGS with more wells. However, the temperature at the BF point or OF point exhibits different variations. Additionally, the temperature at the BF point decreases more rapidly than that at the OF point. In general, an EGS with more fractures is prone to obtain a higher production temperature.

(3) In the fracture length and height directions, heat transportation occurs more quickly in the fracture than in the matrix. However, the cooled rock affected by the fracture channel is limited to the narrow zone surrounding the fracture. The fracture number plays an important role in considering both the heat transportation and the cooling range in a geothermal exploration process. Based on geothermal exploration in the matrix and in the fracture, there is only a slight difference in the heat extraction ratios for the four numerical cases.

CRediT authorship contribution statement

Peng Zhao: Formal analysis, Methodology, Writing – original draft.
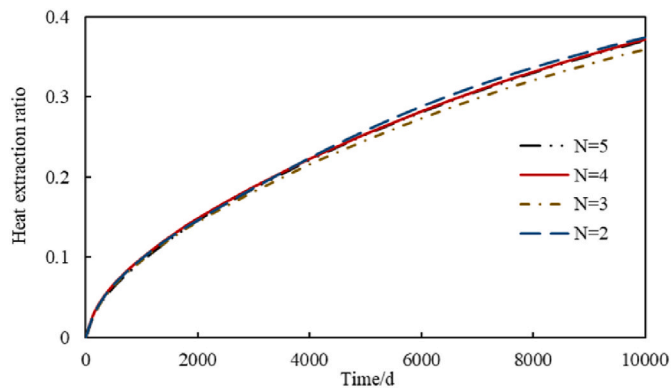**Jun Liu:** Supervision, Conceptualization, Formal analysis, Visualization,

Fig. 16. Effect of fracture number on the heat extraction rate in the EGS.

Writing – original draft. **Derek Elsworth:** Methodology, Writing – review & editing.

Declaration of competing interest

The authors declare that they have no known competing financial interests or personal relationships that could have appeared to influence the work reported in this paper.

Acknowledgements

References

[1] S. Li, S. Wang, H. Tang, Stimulation mechanism and design of enhanced geothermal systems: a comprehensive review, Renew. Sustain. Energy Rev. 155 (2022), 111914.
[2] X. Hu, J. Lv, S. Li, G. Du, Z. Wang, H. Li, H. Zhu, Joint interpretation technology of favorable HDR geothermal resource exploration in Northern Songliao Basin, Unconv. Resour. 2 (2022) 133–138.
[3] W. Kumari, P. Ranjith, Sustainable development of enhanced geothermal systems based on geotechnical research - a review, Earth Sci. Rev. 199 (2019), 102955.
[4] S. Lu, A global review of enhanced geothermal system (EGS), Renew. Sustain. Energy Rev. 81 (2018) 2902–2921.
[5] D. Brown, Recent testing of the HDR reservoir at Fenton Hill New Mexico, Bull. Geoth. Resour. Counc. 22 (9) (1993) 208–214.
[6] C. Xu, P. Dowd, Z. Tian, A simplified coupled hydro-thermal model for enhanced geothermal systems, Appl. Energy 140 (2015) 135–145.
[7] Z. Sun, X. Zhang, Y. Xu, J. Yao, H. Wang, et al., Numerical simulation of the heat extraction in EGS with thermal-hydraulic-mechanical coupling method based on discrete fractures model, Energy 120 (2017) 20–33.
[8] K. Bongole, Z. Sun, J. Yao, Potential for geothermal heat mining by analysis of the numerical simulation parameters in proposing enhanced geothermal system at Bongor basin, Chad, Simulat. Modell. Pract. Theory 107 (2021), 102218.
[9] L. Zhou, Z. Zhu, X. Xie, Y. Hu, Coupled thermal-hydraulic-mechanical model for an enhanced geothermal system and numerical analysis of its heat mining performance, Renew. Energy 181 (2022) 1440–1458.
[10] T. Guo, F. Gong, X. Wang, Q. Lin, Z. Qu, W. Zhang, Performance of enhanced geothermal system (EGS) in fractured geothermal reservoirs with CO2 as working fluid, Appl. Therm. Eng. 152 (2019) 215–230.
[11] T. Guo, Y. Zhang, W. Zhang, B. Niu, J. He, M. Chen, Y. Yu, B. Xiao, R. Xu, Numerical simulation of geothermal energy productivity considering the evolution of permeability in various fractures, Appl. Therm. Eng. 201 (25) (2022), 117756.
[12] Z. Ye, J. Wang, B. Hu, Comparative study on heat extraction performance of geothermal reservoirs with presupposed shapes and permeability heterogeneity in the stimulated reservoir volume, J. Petrol. Sci. Eng. 206 (2021), 109023.
[13] M. Aliyu, H. Chen, Optimum control parameters and long-term productivity of geothermal reservoirs using coupled thermo-hydraulic process modelling, Renew. Energy 112 (2017) 151–165.
[14] X. Song, Y. Shi, G. Li, R. Yang, G. Wang, R. Zheng, J. Li, Z. Lyu, Numerical simulation of heat extraction performance in enhanced geothermal system with multilateral wells, Appl. Energy 218 (2018) 325–337.
[15] M. Aliyu, R. Archer, A thermo-hydro-mechanical model of a hot dry rock geothermal reservoir, Renew. Energy 176 (2021) 475–493.
[16] J. Zinsalo, L. Lamarche, J. Raymond, Design and optimization of multiple wells layout for electricity generation in a multi-fracture enhanced geothermal system, Sustain. Energy Technol. Assessments 47 (2021), 101365.
[17] P. Yu, D. Dempsey, R. Archer, A three-dimensional coupled thermo-hydro-mechanical numerical model with partially bridging multi-stage contact fractures in horizontal-well enhanced geothermal system, Int. J. Rock Mech. Min. Sci. 143 (2021), 104787.
[18] S. Han, Y. Cheng, Q. Gao, C. Yan, J. Zhang, Numerical study on heat extraction performance of multistage fracturing Enhanced Geothermal System, Renew. Energy 149 (2020) 1214–1226.
[19] D. Wang, Y. Dong, Y. Li, Y. Wang, Y. Li, H. Liu, W. Zhang, D. Sun, B. Yu, Numerical simulation of heat recovery potential of hot dry rock under alternate temperature loading, Unconv. Resour. 2 (2022) 170–182.
[20] M. Aliyu, R. Archer, Numerical simulation of multifracture HDR geothermal reservoirs, Renew. Energy 164 (2021) 541–555.
[21] K. Pruess, Enhanced geothermal systems (EGS) using CO2 as working fluid-A novel approach for generating renewable energy with simultaneous sequestration of carbon, Geothermics 35 (2006) 351–367.
[22] L. Zhang, J. Ezekiel, D. Li, J. Pei, S. Ren, Potential assessment of CO2 injection for heat mining and geological storage in geothermal reservoirs of China, Appl. Energy 122 (2014) 237–246.
[23] F. Sun, Y. Yao, G. Li, X. Li, Performance of geothermal energy extraction in a horizontal well by using CO2 as the working fluid, Energy Convers. Manag. 171 (2018) 1529–1539.
[24] K. Bongole, Z. Sun, J. Yao, A. Mehmood, Y. Wang, J. Mboje, Y. Xin, Multifracture response to supercritical CO2-EGS and water-EGS based on thermo-hydromechanical coupling method, Int. J. Energy Res. 43 (2019) 7173–7196.
[25] K. Kim, J. Kemeny, M. Nickerson, Effect of rapid thermal cooling on mechanical rock properties, Rock Mech. Rock Eng. 47 (6) (2014) 2005–2019.
[26] S. Shao, P. Wasantha, P. Ranjith, Effect of cooling rate on the mechanical behavior of heated Strathbogie granite with different grain sizes, Int. J. Rock Mech. Min. Sci. 70 (9) (2014) 381–387.
[27] P. Jin, Y. Hu, J. Shao, G. Zhao, X. Zhu, C. Li, Experimental study on physico-mechanical and transport properties of granite subjected to rapid cooling, Chin. J. Rock Mech. Eng. 37 (11) (2018) 2556–2564 (in Chinese).
[28] P. Siratovich, M. Villeneuve, J. Cole, B. Kennedy, F. Bégué, Saturated heating and quenching of three crustal rocks and implications for thermal stimulation of permeability in geothermal reservoirs, Int. J. Rock Mech. Min. Sci. 80 (2015) 265–280.
[29] F. Yang, G. Wang, D. Hu, Y. Liu, H. Zhou, X. Tan, Calibrations of thermo-hydro-mechanical coupling parameters for heating and water-cooling treated granite, Renew. Energy 168 (2021) 544–558.
[30] F. Zhang, J. Zhao, D. Hu, F. Skoczylas, J. Shao, Laboratory investigation on physical and mechanical properties of granite after heating and water-cooling treatment, Rock Mech. Rock Eng. 51 (2018) 677–694.
[31] F. Kang, T. Jia, Y. Li, J. Deng, C. Tang, X. Huang, Experimental study on the physical and mechanical variations of hot granite under different cooling treatments, Renew. Energy 179 (2021) 1316–1328.
[32] W. Zhang, T. Guo, Z. Qu, Z. Wang, Research of fracture initiation and propagation in HDR fracturing under thermal stress from meso-damage perspective, Energy 178 (2019) 508–521.
[33] Z. Cheng, B. Xi, X. Yang, S. He, X. Li, Experimental study on the evolution on granite permeability under thermal shock, J. Taiyuan Univ. Technol. 52 (2) (2021) 198–203 (in Chinese).
[34] L. Zhang, W. Zhang, J. He, T. Guo, Z. Qu, X. Mou, Study on meso damage and seepage enhancement mechanism of high temperature rocks under rapid cooling, Prog. Geophys. 37 (2) (2022) 551–560 (In Chinese).
[35] J. Liu, L. Xie, B. He, P. Zhao, H. Ding, Performance of free gases during the recovery enhancement of shale gas by CO2 injection: a case study on the depleted Wufeng–Longmaxi shale in northeastern Sichuan Basin, China, Petrol. Sci. 18 (2) (2021) 530–545.
[36] Y. Zhao, Z. Feng, D. Yang, W. Liang, THM (Thermo-hydro-mechanical) coupled mathematical model of fractured media and numerical simulation of a 3D enhanced geothermal system at 573 K and buried depth 6000-7000 M, Energy 82 (2015) 193–205.
[37] B. Liang, H. Jiang, J. Li, C. Gong, A systematic study of fracture parameters effect on fracture network permeability based on discrete-fracture model employing Finite Element Analyses, J. Nat. Gas Sci. Eng. 28 (2016) 711–722.
[38] B. Bai, One-dimensional thermal consolidation characteristics of geotechnical media under non-isothermal condition, Eng. Mech. 22 (5) (2005) 186–191 (in Chinese).
[39] H. Murphy, J. Tester, C. Grigsby, R. Potter, Energy extraction from fractured geothermal reservoirs in Low-Permeability Crystalline Rock, J. Geophys. Res. 86 (B8) (1981) 7145–7158.
[40] M. White, R. Podgorney, S. Kelkar, G. McClure, G. Danko, et al., Benchmark Problems of the Geothermal Technologies Office Code Comparison Study, 2016. Richland, WA (United States).